RSC Advances

ROYAL SOCIETY OF CHEMISTRY

www.rsc.org/advances

Journal Name

ARTICLE

Intrinsic and Extrinsic Proton Conductivity in Metal-Organic Frameworks†

S. Tominaka,[a,b]* and A. K. Cheetham[a]*

Metal-organic frameworks (MOFs), a new class of solid-state materials, have recently been investigated as proton conductors, but little is known about their mechanisms. Since most of the conductivities reported so far were measured using powder samples, there is uncertainty as to whether they exhibit intrinsic proton transport through frameworks and/or micropores, or extrinsic transport through interparticle phases. Herein, we re-visit ferrous oxalate dihydrate $[Fe(ox)(H_2O)_2]$ (ox = oxalate anion), which is a dense MOF and recognized as a model system for MOF-based proton conductors. By single-crystal measurements using microelectrodes, we show that protons do not transport through the crystals ($<10^{-9}$ S cm^{-1}), but that the conductivity observed in powder samples originates from interparticle phases. This result raises a question as to how general is this phenomenon? We have comprehensively surveyed the literature on solid-state proton conductors and found that large numbers of MOFs, including $[Fe(ox)(H_2O)_2]$, have similar activation energy to those of gels and interparticle conductors in classical solid-state materials. This indicates a considerable contribution from interparticle phases towards proton conductivity in MOFs, and single crystal analysis or special methods for powder analysis are clearly necessary to confirm intrinsic conductivity.

Solid-state ion conductors are of great importance for the development of fuel cells, batteries and supercapacitors.[1] A variety of solid-state materials, such as polymers, inorganic materials, and, recently, metal-organic frameworks (MOFs), have been explored for this application. MOFs are a new class of solid-state materials, comprising metal ions and organic ligands that are linked to form one-dimensional to three-dimensional structures.[2, 3] Porous MOFs have attract considerable attention in view of their potential applications in gas sorption, carbon dioxide trapping and catalysis.[2] Since the pores can trap proton carrier molecules as well as accommodating modifications of the walls, these porous MOFs have also been investigated as proton conductors,[4-6] especially for anhydrous conduction.[7, 8] Dense MOFs,[9] which do not have pores that can trap proton carriers, are more analogous to the classical inorganic proton conductors, and protons are expected to be transported through the crystal lattice via defects.

The most extensively studied polymer electrolyte, Nafion, was invented more than 50 years ago, but its proton conduction mechanism is still unclear, mainly due to its complicated ionic channel structure.[10, 11] Compared with that situation, the mechanism in MOFs should be more straightforward, because their detailed crystal structures can be determined by diffraction methods. However, even though a number of proton conductive MOFs have been reported, they need further experimental and theoretical analysis in order to establish a better understanding of their conduction mechanisms. In particular, single-crystal conductivity measurements are necessary to clarify whether protons are transported through the lattice and/or micropores or through interparticle phases. Such interparticle conduction is often observed in inorganic proton conductors and can show conductivities of $>10^{-3}$ S cm^{-1} at room temperature (RT).[12] Thus, it is reasonable to consider whether it contributes to, or even dominates, proton conduction in some of the MOFs.

In the present work we revisit a well-known, proton conductive dense MOF: ferrous oxalate dihydrate $[Fe(ox)(H_2O)_2]$ (ox = oxalate anion). This dense MOF shows an excellent conductivity of 1.3 x 10^{-3} S cm^{-1} (at 25°C and 98% relative humidity (RH)),[13] and is regarded as an outstanding example of MOF-based proton conductors.[4] However, it is unclear whether protons are transported through the framework or not because the data were obtained from a polycrystalline pellet.[13] Here we investigate the conductivity of $[Fe(ox)(H_2O)_2]$ by single crystal methods using microelectrodes,[14] in order to acquire a better understanding of MOF-based proton conductors and this system in particular.

Results and discussion

We synthesized two types of [Fe(ox)(H₂O)₂] crystals; one form comprises high quality single-crystalline prisms (**1**) while the other comprises prisms with a significant level of stacking faults (**2**) (which is typical for [Fe(ox)(H₂O)₂]).[15, 16] **1** was synthesized by annealing out the stacking faults in **2** at 90°C. The crystal structures were determined by single crystal X-ray diffraction, and phase purity was confirmed by powder diffraction (Fig. 1a). Both have [Fe(ox)(H₂O)₂] chains along the long axis of the prisms (i.e., along the *b* axis, determined by diffraction, Fig. 1b), though **2** has stacking faults along the *c** axis according to the streaks observed in the reciprocal lattice (inset in Fig. 1a, and Fig. S1). The different domains are shifted by 50% along the *a* or *b* axes (Figs. 1c, 1d and S2). The unit cell is similar in both cases, except for a 1.2% expansion of the *a* axis in **2**; **1** [*a* = 12.065(12) Å, *b* = 5.559(2) Å, *c* = 9.817(9) Å, *β* = 128.03(15)° at 293 K] and **2** [*a* = 12.209(4) Å, *b* = 5.5526(7) Å, *c* = 9.865(3) Å, *β* = 128.20(6)° at 297 K]. Compared with the reported data [*a* = 12.011(11) Å, *b* = 5.557(5) Å, *c* = 9.920(9) Å, *β* = 128.53(3)° at 293 K],[16] **1** has a 0.4% longer *a* axis and a 1.0% shorter *c* axis (Table S1). These differences are attributable to the low quality of the single crystal data of **1** due to twinning; the lattice constants obtained by Pawley fitting of the powder X-ray data agree well with the reported values (Fig. S3 and Table S1).
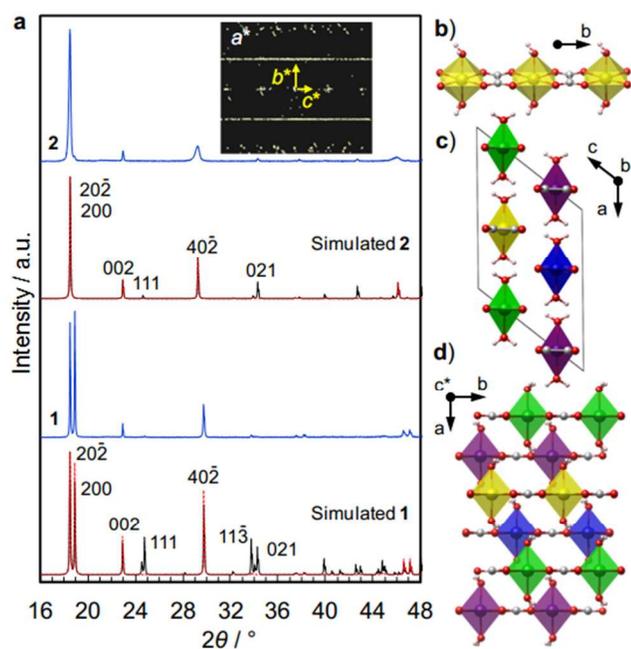
tetrathiafulvalene nitrate crystal (Fig. S4).[14] A tiny deep red crystal was placed on two gold microelectrodes having a 80 μm gap (Fig. 2a, inset), and a semicircle, whose diameter can be assigned to resistance of the material (1.1 kΩ cm), was obtained. This confirms the reliability of the conductivity measurements using the microelectrode method. Figure 2b shows impedance spectra of **1**, measured along the *b* axis of the crystal, i.e., along the [Fe(ox)(H₂O)₂] chains. The resistance is >10¹¹ Ω, and slightly decreases with increasing humidity. As shown in the inset, **1**, **2** and the blank cell have almost the same resistance, indicating that the conductivity originates from the quartz surface, not from [Fe(ox)(H₂O)₂]. In addition, the spectra of **1**, **2** and the blank cell are similar (Fig. S5), confirming that the large resistances are attributable to the bulk of the materials, not to the contact between the materials and the electrodes. The proton conductivity through the [Fe(ox)(H₂O)₂] framework is judged to be <<5.4 × 10⁻⁹ S cm⁻¹ (20°C, 80%RH) for **1**. In other words, it is an insulator. The discussion on the hydrogen bond networks also supports the conclusion (Fig. S6).

Figure 1 Crystallographic analyses on the [Fe(ox)(H₂O)₂] samples. (a) PXRD patterns of two [Fe(ox)(H₂O)₂] samples: **1** is single crystalline, and **2** contains stacking faults. The black lines show simulated PXRD patterns, and the red dotted lines show simulated PXRD patterns with 010 preferred orientation. The inset image shows the reciprocal lattice images along the *a** direction. b-d, Structure images. The FeO₆ octahedra are connected by oxalate along the *b* axis (b). The unit cell is composed of 4 different [Fe(ox)(H₂O)₂] chains (c, d). The stacking faults in **2** are indicated to be along the *c** axis.

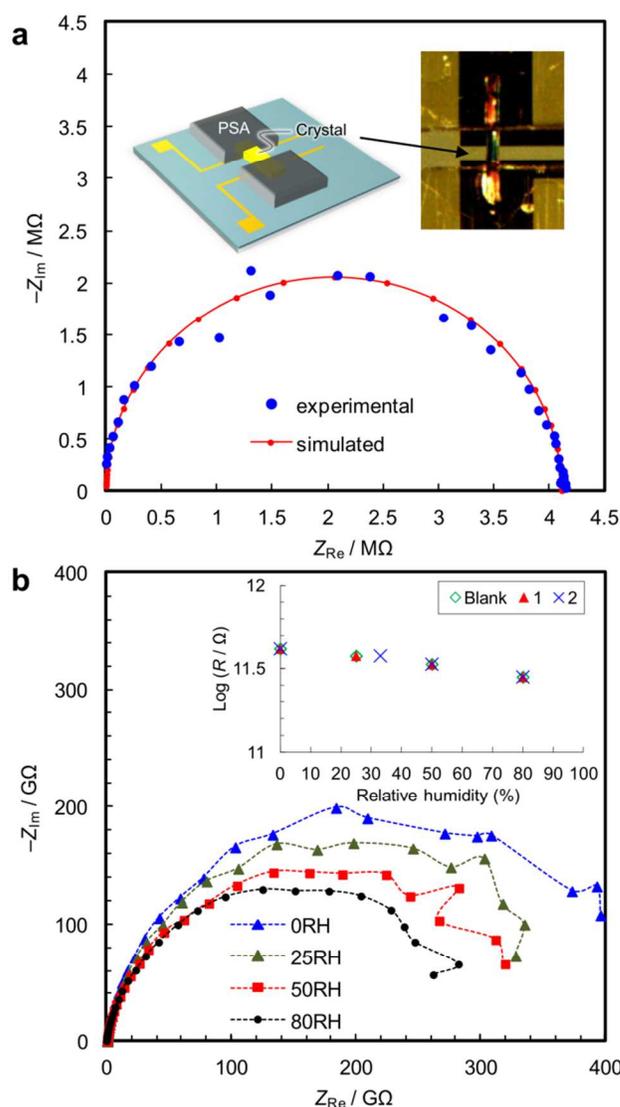Figure 2a shows the single-crystal impedance set-up and demonstrates its performance for an electrically conductive

Figure 2 Single-crystal impedance analyses. (a) Complex-plane impedance data for a tetrathiafulvalene nitrate crystal (42 μm wide × 4 μm thick) were collected in order to demonstrate the microelectrode method. The inset image illustrates the setup, and shows a crystal contacted with microelectrodes having a 80 μm gap using a pressure sensitive adhesive, PSA. The conductivity along the *a* axis of the crystal was measured. The data were analyzed using an equivalent circuit consisting of the parallel combination of a resistance and a capacitance. (b) Complex-plane impedance diagrams for a single crystal of **1** at room temperature under different relative humidities. The inset compares resistance vs. relative humidity of **1** (23 μm wide × 23 μm thick), **2** (26 μm wide × 26 μm thick) and the blank cell. The measurements were performed along the *b* axis of the crystal, which was confirmed by X-ray diffraction.

We then carried out conductivity measurements of **1** and **2** using powder samples under saturated water vapour (Fig. S7-S9). The conductivity values are 5.7×10^{-4} S cm^{-1} for **1** and 1.5×10^{-3} S cm^{-1} for **2** at 20 °C (dry samples, $<10^{-12}$ S cm^{-1}); these are in good agreement with the previous measurements.[16] The Arrhenius plots (Fig. 3) show that proton conduction of **1** proceeds via a constant mechanism in the range 20–90°C, as indicated by the linear relationship (activation energy, $E_a = 0.17$ eV, and pre-exponential factor, $\sigma_0 = 1.5 \times 10^2$ S cm^{-1} K^{-1}). **2** has similar kinetics in the range 20–60°C ($E_a = 0.14$ eV and $\sigma_0 = 1.2 \times 10^2$ S cm^{-1} K^{-1}), but the gradient decreases at higher temperatures, indicating that some change has taken place. This is most likely due to the annealing out of the stacking faults which takes place in this temperature range. The E_a values are close to those for proton conduction in liquids,[17] $E_a = \sim 0.1$ eV.[18] In our opinion, therefore, the protons are transported through an aqueous phase that is formed between the particles. Since the solubility of [Fe(ox)(H$_2$O)$_2$] is negligible (Supporting Information), the protons must be released from the particle surface. This is consistent with the Gouy-Chapman Theory of diffuse layers,[19] which shows that protons can exist as far away as ~900 nm from fixed counter anions.[20]
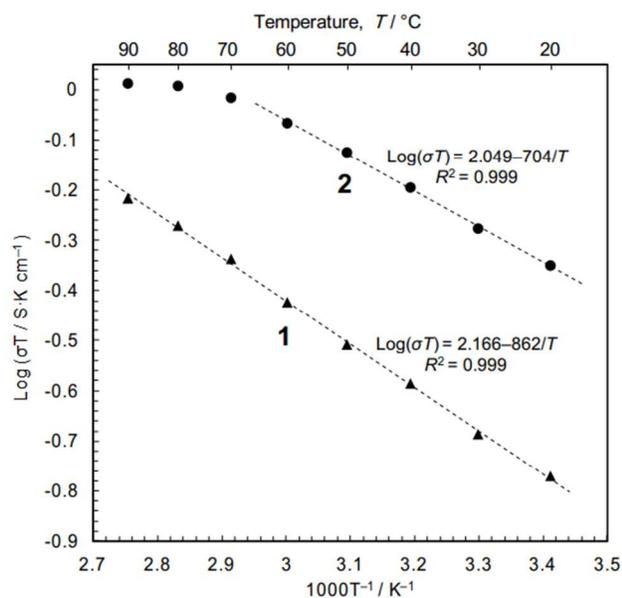
In order to explore the generality of interparticle conduction, we have surveyed the literature on proton conductors more widely. Figure 4 compares σ_0 vs. E_a for proton conductivity in MOFs in comparison with classical solid-state materials (details are available in the Supporting Information; Table S2-S4 and Fig. S10). We can classify them into two types on the basis of their activation energies: type 1 has $E_a <0.4$ eV, and type 2 has $E_a >0.5$ eV. In classical solid-state materials, most of the gels, polymer electrolytes and interparticle conductors are type 1, while most of anhydrous or microporous conductors are type 2. The exception is the anhydrous conductor, CsHSO$_4$, which has significant rotational disorder of SO$_4$, and thus protons can move as in a liquid.[21]
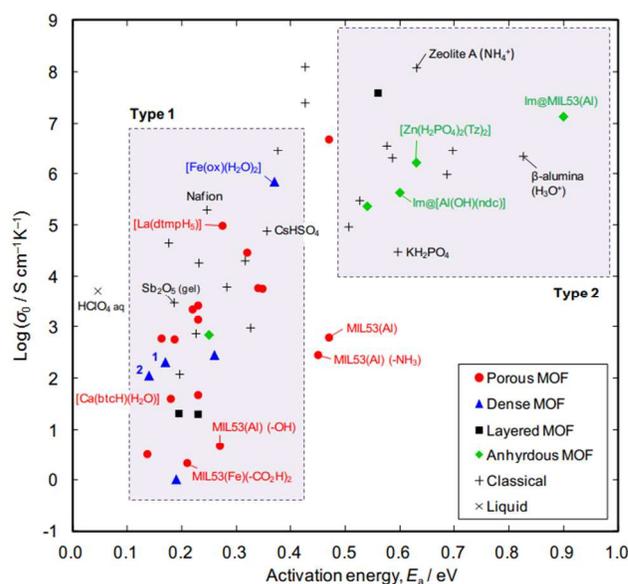

Figure 4 Comparison of proton conductivity in metal-organic frameworks (MOFs) and classical solid-state materials. The relationship between the pre-exponential factor σ_0 of the Arrhenius Equation and the activation energy E_a are plotted. MIL53(M) is [M(OH)(14bdc)], where bdc is benzenedicarboxylate anion. Im@ refers to the incorporation of imidazole. -NH$_3$, -OH and -CO$_2$H correspond to functional groups of modified bdc molecules. ndc = 1,4-naphthalenedicarboxylate anion. btc = 1,3,5-benzenetricarboxylate anion. Tz = 1,2,4-triazole. dtmp = hexamethylenediamine tetramethylenephosphonate anion.

Figure 3 Arrhenius plots of the proton conductivity in [Fe(ox)(H$_2$O)$_2$] **1** and **2** obtained by powder impedance analyses. The AC impedance data were obtained at different temperatures under saturated water vapour.

From the extensive studies of classical hydrated proton conductors, such as Nafion, we can establish some fundamental aspects of proton conduction in hydrated MOFs. Nafion has 18–35 Å water nanochannels (11 wt% H$_2$O) lined by –SO$_3$H groups at separations of ~8 Å.[10, 22] With dehydration, the channel becomes narrower (<10 Å), and E_a increases up to 0.4–0.5 eV due to the influence of the walls.[17] This high E_a can be accounted for by the restriction of the molecular dynamics in nanopores, because the diffusion of molecules in nanopores becomes slower than in the bulk when the pores are smaller than about ten molecular diameters;[23] furthermore, the Grotthuss Mechanism does not operate due to the lack of a long-range hydrogen bonded network.[24] Such influence of the walls is also observed in microporous materials; for example,

zeolite-A (~4.5 Å aperture) containing NH_4^+ (2.8 Å diameter) with 11 wt% water shows E_a = 0.63 eV.[25]

Compared with these classical materials, the porous MOFs of type 1 have exceptionally low E_a values as if there is no influence of the interior walls. For example, MIL-53 ([M(OH)(bdc)], bdc = 1,4-benzenedicarboxylate anion) has 8.5 Å × 8.5 Å channels,[8, 26] and MIL-53 functionalized with –CO_2H groups shows E_a = 0.21 eV.[6] [Ca(btcH)(H_2O)]·H_2O (btc = 1,3,5-benzenetricarboxylate anion) has <6.4 Å water channels,[27, 28] and shows E_a = 0.18 eV.[29] [La(dtmpH_5)]·7H_2O (dtmp = hexamethylenediamine tetramethylenephosphonate anion) has water channels of <11.7 Å,[28] and shows E_a = 0.28 eV.[30] These low E_a values in microporous MOF materials probably indicates the presence of interparticle conduction as found in the case of polycrystalline [Fe(ox)(H_2O)$_2$]. Thus, we would argue that the observed conductivities are probably extrinsic rather than intrinsic.

By contrast, most of the anhydrous porous MOFs containing heterocycles (i.e., imidazole and triazole) as guest carriers are in type 2. For example, MIL-53 containing guest imidazole molecules (4.3 Å × 3.7 Å) has E_a of 0.9 eV[8] (while free imidazole and imidazole in polymer electrolytes have a lower E_a of 0.25 eV)[31]. We speculate that the high E_a of the former points to some influence from pore walls and thus the conductivities of these anhydrous MOFs are probably due to intrinsic mobility through the micropores. Another example of an intrinsic conductor is the anhydrous, dense MOF, [Zr(HPO$_4$)$_2$(Tz)$_2$] (Tz = 1,2,4-triazole), whose conductivity was the same for both single crystal and powder samples.[32] In the light of the present work, we regard this material as an analogue of KH_2PO_4 and the high E_a is probably due to the unsuitable hydrogen bond lengths.[33]

In order to be certain of obtaining reliable data, we propose that one should measure the conductivity using single crystal samples. Whenever powder samples are used, it is hard to remove the influence of interparticle phases, especially in hydrated conductors. In addition, there is further concern about the reliability with powders due to the possibility of phase transitions associated with the pelletizing pressure. The impact of the pelletizing process is often underestimated, but can be very important in yielding reproducible results.[34] The pressure needed for making a stable pellet form of a MOF, e.g., 0.2–0.5 GPa in our own experience, might be too high for some MOFs to retain the original structure of interest. For example, MIL-53(Cr) undergoes a phase transition at around 55 MPa,[35] zinc imidazolate undergoes phase transition in the range 0.54–0.85 GPa,[36] [Zn$_4$O(14bdc)$_3$] (MOF-5) is amorphized at 3.5 MPa,[37] and an erbium formate framework undergoes a phase transition at 0.6 GPa.[38] It is better not to pelletize porous MOFs but to prepare the sample using milder methods, as was done for Im@MIL53;[8] PXRD patterns should also be checked after the measurements. We confirmed that 0.5 GPa does not change the crystal structure of the dense framework of [Fe(ox)(H_2O)$_2$]. We believe that the difference between our powder results and the previously reported ones (E_a = 0.37 eV and σ_0 = 10^6 S cm^{-1} K^{-1}

at 98%RH)[13] is due to the pelletization procedure or the RH difference.

Conclusions

On the basis of experimental evidence and a literature survey, it is proposed that hydrated interparticle phases make a considerable contribution to proton conduction in many MOFs when measurements are made on pellets. MOFs are quite new materials in terms of the history of proton conductors, and the next stage in this area is to acquire a better understanding of proton conduction mechanisms in such systems.

Methods

Synthesis. Diethyl oxalate (1 mmol; Aldrich, >99%) and iron sulfate heptahydrate (2 mmol; Aldrich, >99%) were dissolved in 20 mL of distilled water.[16] The solution was heated by microwave radiation (Biotage Initiator) at 90°C for 2 h, slowly cooled down to room temperate, and then aged overnight. These crystals, **2** (yield = 72%, oxalate-base), were further treated in the mother solution at 90°C for 3 days, **1** (yield = 82%). Yellow prisms (10-100 μm thick and 100-1000 μm long) were recovered by vacuum filtration and rinsed with distilled water.

The chemical compositions were determined by elemental analysis at the Department of Chemistry, University of Cambridge (found, calcd.), for $C_2H_4O_6Fe$: C (13.31, 13.35), H (2.20, 2.22), N (0.00, 0.00) for **1**; C (13.34, 13.35), H (2.12, 2.22), N (0.00, 0.00) for **2**. The H_2O content was determined by thermal analysis (Fig. S11) (found, calcd.): **1** (21.4, 20.0), **2** (20.4, 20.0).

Structure determinations. The crystal structures were determined at room temperature by single crystal diffractometry using an Oxford Diffraction Gemini A Ultra X-ray diffractometer with Mo Kα radiation. The structure was solved by direct methods and then refined by the least squares methods using the SHELX program[39] within the Olex2 interface.[40] All non-hydrogen atoms were refined anisotropically and hydrogen atoms were refined isotropically. Hydrogen atoms on water molecules were then added to calculated positions. Visualization of structures was carried out using the VESTA program.[41] CIF files are available (CCDC 1010845-1010846).

The phase purity was confirmed by powder X-ray diffraction (PXRD). The PXRD data were collected using a Bruker-AXS D8 diffractometer with Cu Kα radiation in the Bragg–Brentano geometry. The patterns were analyzed by the Pawley method using the GSAS-II software,[42] and plotted with zero-shift correction and background subtraction. The PXRD patterns were simulated using the Mercury program[43] with the March-Dollase parameter[44] of 3.0 for modeling the influence of preferred orientation. For the simulations, the high quality crystallographic structure reported by Echigo et al. was used for **1**,[16] and the crystallographic information obtained by single crystal diffraction in the present work was used for **2**.

Single-crystal impedance measurements. The single-crystal impedance measurements are carried out by mounting the crystal on a quartz chip having microelectrodes with a 80 μm gap (Fig. 2a, inset).[14] Humidity was controlled by mixing water-saturated nitrogen gas and dry nitrogen gas, and AC impedance spectra were collected after an equilibration time of >6 h. The conductivity was measured by the AC impedance method using a Gamry Interface1000 electrochemical instrument in the frequency range of 1 MHz to 10 mHz at an AC amplitude of 100 mV. The crystallographic orientations of the samples were checked using the single-crystal diffractometer.

Powder impedance measurements. The crystals (100–130 mg) were gently ground using a pestle and mortar, and then pelletized (1 cmϕ, ~0.6 mm thick) at 0.5 GPa for 5 min with a few drops of water. The data were collected by keeping the pellets in a closed cell containing saturated water vapour. After equilibration at 90°C for a few days, impedance spectra were collected at every 10°C from 90°C to 20°C with an equilibration time of >8 h. The reproducibility was confirmed using different pellets prepared in the same way.

Infrared spectroscopy. Fourier-transform infrared spectroscopy (FTIR) was carried out using a Bruker Tensor 27 infrared spectrometer with a diamond attenuated total reflectance (ATR) attachment. The data were collected in the wavenumber range from 520 to 4000 cm^{-1} at room temperature.

Acknowledgements

Notes and references

^{a}Department of Materials Science and Metallurgy, University of Cambridge, Charles Babbage Road, Cambridge CB3 0FS, United Kingdom. Fax: +44 1223 334567; Tel: +44 (0)1223 767061; E-mail: akc30@cam.ac.uk.
^{b}International Center for Materials Nanoarchitectonics (WPI-MANA), National Institute for Materials Science (NIMS), Ibaraki 305-0044, Japan. Tel: +81 (0)29 860 4594; E-mail: TOMINAKA.Satoshi@nims.go.jp
†Electronic Supplementary Information (ESI) available: [experimental details, crystallographic analysis, cif files, thermogravimetric analysis, infrared spectra]. See DOI: 10.1039/b000000x/

1. P. G. Bruce, ed., *Solid State Electrochemistry*, Cambridge University Press, Cambridge, 1995.
2. H. Furukawa, K. E. Cordova, M. O'Keeffe and O. M. Yaghi, *Science*, 2013, **341**, 974.
3. A. K. Cheetham, C. N. R. Rao and R. K. Feller, *Chem. Commun.*, 2006, 4780-4795; M. Eddaoudi, J. Kim, N. Rosi, D. Vodak, J. Wachter, M. OÕKeeffe and O. M. Yaghi, *Science*, 2002, **295**, 469-472.
4. M. Yoon, K. Suh, S. Natarajan and K. Kim, *Angew. Chem. Int. Ed.*, 2013, **52**, 2688-2700.
5. P. Ramaswamy, N. E. Wong and G. K. H. Shimizu, *Chem. Soc. Rev.*, 2014, **43**, 5913-5932.
6. A. Shigematsu, T. Yamada and H. Kitagawa, *J. Am. Chem. Soc.*, 2011, **133**, 2034-2036.
7. J. A. Hurd, R. Vaidhyanathan, V. Thangadurai, C. I. Ratcliffe, I. L. Moudrakovski and G. K. H. Shimizu, *Nature Chem.*, 2009, **1**, 705-710.
8. S. Bureekaew, S. Horike, M. Higuchi, M. Mizuno, T. Kawamura, D. Tanaka, N. Yanai and S. Kitagawa, *Nature Mater.*, 2009, **8**, 831-836.
9. A. K. Cheetham and C. N. R. Rao, *Science*, 2007, **318**, 58-59.
10. K. Schmidt-Rohr and Q. Chen, *Nature Mater.*, 2008, **7**, 75-83.
11. K. A. Mauritz and R. B. Moore, *Chem. Rev.*, 2004, **104**, 4535-4585.
12. G. Alberti and M. Casciola, in *Proton conductors: Solids, membranes and gels (materials and devices)*, ed. P. Colomban, Cambridge University Press, Cambridge, 1992, pp. 238-253; S. Tominaka, N. Akiyama, F. Croce, T. Momma, B. Scrosati and T. Osaka, *J. Power Sources*, 2008, **185**, 656-663; P. Colomban and A. Novak, in *Proton conductors: Solids, membranes and gels (materials and devices)*, ed. P. Colomban, Cambridge University Press, Cambridge, 1992, pp. 272-293.
13. T. Yamada, M. Sadakiyo and H. Kitagawa, *J. Am. Chem. Soc.*, 2009, **131**, 3144-3145.
14. S. Tominaka, S. Henke and A. K. Cheetham, *CrystEngComm*, 2013, **15**, 9400-9407.
15. J. Dubernat and H. Pezerat, *J. Appl. Cryst. (French)*, 1974, **7**, 387-393.
16. T. Echigo and M. Kimata, *Phys. Chem. Miner.*, 2008, **35**, 467-475.
17. M. Eikerling and A. A. Kornyshev, *J. Electroanal. Chem.*, 2001, **502**, 1-14.
18. P. Colomban and A. Novak, in *Proton conductors: Solids, membranes and gels (materials and devices)*, ed. P. Colomban, Cambridge University Press, Cambridge, 1992, pp. 38-60.
19. A. J. Bard and L. R. Faulkner, in *Electrochemical methods: fundamentals and applications*, John Wiley & Sons, Inc, New York, 2001, pp. 534-554.
20. S. Tominaka, C.-W. Wu, K. Kuroda and T. Osaka, *J. Power Sources*, 2010, **195**, 2236–2240.
21. P. Colomban and A. Novak, in *Proton Conductors: Solids, Membranes and Gels - Materials and Devices*, ed. P. Colomban, Cambridge University Press, Cambridge, 1992, pp. 165-182.
22. S. J. Paddison and R. Paul, *Phys. Chem. Chem. Phys.*, 2002, **4**, 1158-1163.
23. S. T. Cui, *J. Chem. Phys.*, 2005, **123**, 054706.
24. K. D. Kreuer, A. Rabenau and W. Weppner, *Angew. Chem. Int. Ed.*, 1982, **21**, 208-209.
25. K. D. Kreuer, W. Weppner and A. Rabenau, *Mat. Res. Bull.*, 1982, **17**, 501-509.
26. G. Férey, *Che. Soc. Rev.*, 2008, **37**, 191-214; C. Serre, F. Millange, C. Thouvenot, M. Nogues, G. Marsolier, D. Louer and G. Férey, *J. Am. Chem. Soc.*, 2002, **124**, 13519-13526.
27. M. J. Plater, R. A. Howie and A. J. Roberts, *Chem. Commun.*, 1997, 1151-1151; A. L. Spek, *Acta Cryst. Sec. D*, 2009, **65**, 148-155.

RSC Advances Accepted Manuscript

28. Calculated using the Platon software.

29. A. Mallick, T. Kundu and R. Banerjee, *Chem. Commun.*, 2012, **48**, 8829-8831.

30. R. M. P. Colodrero, P. Olivera-Pastor, E. R. Losilla, M. A. G. Aranda, L. Leon-Reina, M. Papadaki, A. C. McKinlay, R. E. Morris, K. D. Demadis and A. Cabeza, *Dalton Trans.*, 2012, **41**, 4045-4051.

31. K. D. Kreuer, A. Fuchs, M. Ise, M. Spaeth and J. Maier, *Electrochim. Acta*, 1998, **43**, 1281-1288.

32. D. Umeyama, S. Horike, M. Inukai, T. Itakura and S. Kitagawa, *J. Am. Chem. Soc.*, 2012, **134**, 12780-12785.

33. A. Potier, in *Proton conductors: Solids, membranes and gels (materials and devices)*, ed. P. Colomban, Cambridge University Press, Cambridge, 1992, pp. 1-17.

34. P. J. Beldon, S. Tominaka, P. Singh, T. S. Dasgupta, E. G. Bithell and A. K. Cheetham, *Chem. Commun.*, 2014, **50**, 3955-3957.

35. I. Beurroies, M. Boulhout, P. L. Llewellyn, B. Kuchta, G. Férey, C. Serre and R. Denoyel, *Angew. Chem. Int. Ed.*, 2010, **49**, 7526-7529.

36. E. C. Spencer, R. J. Angel, N. L. Ross, B. E. Hanson and J. A. K. Howard, *J. Am. Chem. Soc.*, 2009, **131**, 4022-4026.

37. Y. H. Hu and L. Zhang, *Phys. Rev. B*, 2010, **81**, 174103.

38. E. C. Spencer, M. S. R. N. Kiran, W. Li, U. Ramamurty, N. L. Ross and A. K. Cheetham, *Angew. Chem. Int. Ed.*, 2014, **53**, 5689-5692.

39. G. M. Sheldrick, *Acta Cryst. Sec. A*, 2008, **64**, 112-122.

40. O. V. Dolomanov, L. J. Bourhis, R. J. Gildea, J. A. K. Howard and H. Puschmann, *J. Appl. Cryst.*, 2009, **42**, 339-341.

41. K. Momma and F. Izumi, *J. Appl. Cryst.*, 2011, **44**, 1272-1276.

42. B. H. Toby and R. B. Von Dreele, *J. Appl. Cryst.*, 2013, **46**, 544-549.

43. C. F. Macrae, I. J. Bruno, J. A. Chisholm, P. R. Edgington, P. McCabe, E. Pidcock, L. Rodriguez-Monge, R. Taylor, J. van de Streek and P. A. Wood, *J. Appl. Cryst.*, 2008, **41**, 466-470.

44. W. A. Dollase, *J. Appl. Cryst.*, 1986, **19**, 267-272.

Intrinsic and Extrinsic Proton Conductivity in Metal-Organic Frameworks

S. Tominaka and A. K. Cheetham

Hydrated interparticle phases are considered to make a considerable contribution to proton conduction in many metal-organic frameworks.